

# Non-centrosymmetric superconductors on honeycomb lattice

Der-Hau Lee<sup>1</sup> and Chung-Hou Chung<sup>1,2</sup>

<sup>1</sup>*Electrophysics Department, National Chiao-Tung University,  
HsinChu, Taiwan, 300, R.O.C.*

<sup>2</sup>*Physics Division, National Center for Theoretical Sciences,  
HsinChu, Taiwan, 300 R.O.C.*

(Dated: March 16, 2018)

We study non-centrosymmetric topological superconductivity in correlated doped quantum spin-Hall insulators (QSHI) on honeycomb lattice without inversion symmetry where the intrinsic (Kane-Mele) and Rashba spin-orbit couplings can in general exist. We explore the generic topologically non-trivial superconducting phase diagram of the model system. Over a certain parameter space, the parity-mixing superconducting state with co-existing spin-singlet  $d+id$  and spin-triplet  $p+ip$ -wave pairing is found. On a zigzag nanoribbon, the parity-mixing superconducting state shows co-existing helical and chiral Majorana fermions at edges. Relevance of our results for experiments is discussed.

PACS numbers: 72.15.Qm, 7.23.-b, 03.65.Yz

## I. INTRODUCTION

Non-centrosymmetric superconductors (NCSs) have drawn intensive attraction since their discoveries in last decade due to the lack of space inversion symmetry, such as  $CePt_3Si$ ,  $UIr$  and  $Li_2Pd_3B$ <sup>1</sup>. Based on Pauli principle, the total electronic wave function is antisymmetric under particle exchange. However, there is no definitely symmetry of spatial wave function in NCS, giving rise to the exotic mixture of spin singlet (with even parity) and triplet states (with odd parity) Cooper pairs. Graphene and graphene-based two-dimensional materials, such as transition metal dichalcogenides (TMDs), silicene, germanene, the binary compounds of the group-IV elements, and the group III.V compounds all have broken inversion symmetry<sup>2</sup>, and are possible candidates of NCS. In particular, TMDs have been studied extensively both theoretically and experimentally for its promising properties in valleytronics and spintronics applications<sup>3-12</sup>, such as: stronger spin-orbit (SO) coupling via  $d$  orbital of the metal atoms in  $MoS_2$ , strong and robust SO interaction in graphene on TMD substrates<sup>13</sup>.

For moving electrons in a closed orbit, an electric field will produce an effective magnetic field via relativistic effect, which generates a Zeeman energy term, recognized as Rashba SO coupling. The electric field based Rashba interaction can be internal in quantum wells with structural inversion symmetry breaking or external as is in graphene<sup>14,15</sup>. Due to Rashba interaction, these systems show non-trivial helical spin textures where spins with the same species rotating with the same chirality at the Fermi surface. Similar spin-momentum-lock phenomena also occur in topological insulators and NCSs<sup>1,16</sup>. Therefore, it is promising to expect the Rashba coupling to be present in NCS. Note that the geometric Berry phase of moving electrons in topological material is associated with the non-trivial Chern number via Kubo formula for Hall conductivity<sup>17</sup>, indicating the existence of topolog-

ically non-trivial properties, such as: gapless metallic edge states in topological insulators (TIs) and Majorana fermions (MFs) as zero-energy charge-neutral edge states of topological superconductors (TSCs)<sup>18-21</sup>.

An interesting aspect of Rashba coupling in NCSs is that it induces spin-triplet pairing (apart from the conventional spin singlet pairing) due to the in-balance in populations of different spin species via Rashba coupling. A non-trivial Chern number has been predicted in spin triplet  $p+ip$  superconductors induced by Rashba interaction on square lattices under strong magnetic fields, which suggests that NCSs are topological superconductors<sup>22</sup>. Similar results have been reported on honeycomb lattice for  $MoS_2$ , which was predicted to support exotic triplet pairing phases<sup>23</sup> and was argued that superconductivity can be induced there experimentally via applying gate voltages<sup>24</sup>.

On the other hand, for doped graphene in the absence of SO couplings, spin-singlet chiral superconducting state with  $d+id$  pairing is energetically favourable as the ground state<sup>25</sup>. It was found that the  $d+id$ -wave state is a state with mixed  $s$ -wave and exotic  $p+ip$ -wave pairing orders at low energy<sup>26</sup>. The chiral nature comes from fact that the two  $d+id$ -wave state carry an equal weight under six fold symmetry of the honeycomb lattice, and a linear combination of two order parameters is needed to describe the system. The chiral superconductivity also leads to breaking of both time-reversal (TR) and parity symmetries. Further investigations confirmed that there are two co-propagating chiral surface states per zigzag graphene nanoribbon (ZGNR) edge, which shows the system is topological non-trivial with Chern number being 2<sup>27</sup>.

Including the intrinsic (Kane-Mele) SO coupling in graphene, exotic and distinct helical topological edge states with two counter-propagating chiral modes protected by the TR symmetry were predicted within the Kane-Mele (KM) model, signature of 2D quantum spin

Hall (topological) insulator<sup>28</sup>. The TR symmetry invariant KM model exhibits a mirror symmetric SO interaction, in contrast to the Rashba SO coupling<sup>18</sup>, and is a perfect theoretical model for TI phases in two dimensions<sup>29</sup>. Recent study further showed an exotic 2D spin-singlet TSC with non-trivial pseudospin Chern number in doped correlated KM model on honeycomb lattice<sup>30</sup>. There, the system undergoes a topological phase transition from a phase with chiral MFs to a phase with helical Majorana zero modes were realized with increasing the intrinsic SO coupling.

The purpose of this paper is to explore all possible topologically non-trivial non-centrosymmetric superconducting states in graphene-based materials by combining all the phenomena mentioned above, including the effects of intrinsic (KM) and Rashba SO couplings, the mixture of  $d+id$  spin singlet and triplet  $p+ip$ -wave pairings in the presence of both KM and Rashba SO couplings. A recent related study on the simplified model without KM interaction in cuprates has shown non-trivial topological properties<sup>32</sup>. However, there is still lack of a comprehensive analysis of the more general and generic model systems for NCS on honeycomb lattice. To realize parity mixing phenomena, experimental setups have been proposed theoretically<sup>32-34</sup>. The corresponding Majorana mode can be detected by Andreev reflection<sup>35</sup> or electrical detection<sup>36</sup> where some signatures of MFs have been observed experimentally in hybrid structures via these approaches<sup>37,38</sup>. The remaining parts of the paper are organized as follows: Section 2 describes computation model and Chern number calculation formula. Section 3 presents main results: the topological phase diagram and corresponding edge spectrum. In this work, we aim for edge states of graphene-based system, which is zigzag nanoribbon (ZNR). Section 4 summarizes results and discusses related issues. Finally, conclusions are provided in Section 5.

## II. THE MODEL

The Rashba and KM SO couplings have been argued to exist in graphene<sup>28</sup>. Both Rashba and KM interactions couple spin-up and spin-down states, and break the SU(2) symmetry. However, the U(1) symmetry still remains for the former, whereas the latter does not<sup>39</sup>.

### A. Rashba spin-orbital interaction

For electric field perpendicular to the graphene plane, the Hamiltonian of Rashba model is represented as<sup>40</sup>

$$H_R = i\lambda_R \sum_{\langle ij \rangle \sigma \sigma'} a_{i\sigma}^\dagger (\tilde{\sigma} \times e_{ij})_z b_{j\sigma'} + h.c.. \quad (1)$$

Here,  $a(b)$  stand for sublattices A(B),  $a_{i\sigma}^\dagger (b_{j\sigma'})$  is a creation (an annihilation) operator for an electron at site

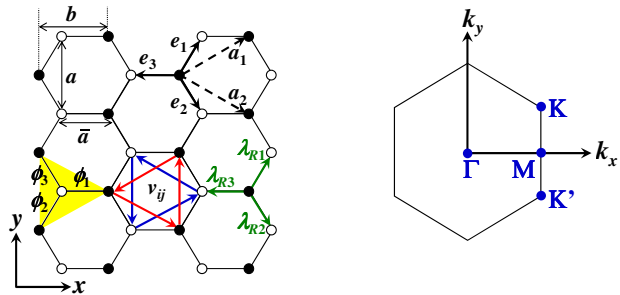


FIG. 1. (Left) Plot for honeycomb lattice. (right) Corresponding first Brillouin zone with the two inequivalent Dirac points  $K$  and  $K'$  and high symmetry points  $\Gamma$  and  $M$ . The honeycomb lattice consists of two interpenetrating triangular lattices denoted by sublattice A (dark circles) and sublattice B (open circles) with lattice vectors  $a_1$  and  $a_2$  (dashed arrows). The nearest-neighbor lattice vectors between nearest-neighbor A and B sites are denoted by  $e_{i=1,2,3}$  with site-site distance  $\bar{a}$  and lattice constant  $a = \sqrt{3}\bar{a}$ . Here,  $\bar{a}$  is set to be 1.  $b$  is used to label the location of individual zigzag chain along  $x$  axis. The red (blue) arrows within sublattice A(B) represent the directions of the next-nearest-neighbor hopping term of Kane-Mele model. The green arrows indicate the spin dependent interaction of Rashba model, and shaded yellow triangle represents amplitudes of the superconducting pairing gaps (see text).

$i(j)$  with spin  $\sigma$  ( $\sigma'$ ). The Pauli matrix is defined as  $\tilde{\sigma} = (\sigma_x, \sigma_y, \sigma_z)$ .  $\lambda_R$  is the Rashba coupling. The nearest-neighbor (NN) vectors of the honeycomb lattice are given by:  $(1/2, \sqrt{3}/2)$ ,  $(1/2, -\sqrt{3}/2)$ , and  $(-1, 0)$ .  $\langle ij \rangle$  denotes NN sites, connected by unit vectors  $e_{ij}$ .  $\lambda_R$  is proportional to the electric field. The explicit Rashba SO terms,  $(\tilde{\sigma} \times e_{ij})_z$ , along three NN vectors,  $e_i$ , can be described by

$$\begin{aligned} \lambda_{R1} &= (\sigma_y - \sqrt{3}\sigma_x)/2, \\ \lambda_{R2} &= (\sigma_y + \sqrt{3}\sigma_x)/2, \\ \lambda_{R3} &= -\sigma_y, \end{aligned} \quad (2)$$

those are illustrated schematically as green lines in figure 1.

The bulk band structure of graphene under Rashba interaction does not open a gap in the spectrum. It exhibits the crossings of conduction and valence bands, giving rise to the splitting of the original dispersion line on the Dirac points. The probability of finding an electron in the spin-up and spin-down state is equal. As a result, the Rashba SO interaction does not break TR symmetry. For the band structure of ZGNR, it has been shown that there is crossing of conduction and valence edge bands, whereas intrinsic SO coupling tend to open gaps. Furthermore, the Rashba SO interaction produces a non-homogeneous spin polarization on the edge states of the ZGNR. This is in contrast to the effect produced by the intrinsic KM SO coupling where spin-polarized states have same spatial spin distribution<sup>40</sup>.

## B. Kane-Mele (intrinsic) spin-orbital interaction

The Kane-Mele SO coupling is represented by the spin dependent next-nearest-neighbor (NNN) hopping, reads<sup>28</sup>

$$H_{KM} = i\lambda_{SO} \sum_{\langle\langle ij \rangle\rangle\sigma} v_{ij}\sigma_z c_{i\sigma}^\dagger c_{j\sigma} + h.c. \quad (3)$$

Here,  $c = a$  or  $b$ .  $\lambda_{SO}$  is the Kane-Mele (intrinsic) spin-orbital coupling.  $\langle\langle ij \rangle\rangle$  denotes NNN sites. For the same sublattice hopping, amplitude  $v_{ij} = 1$  or  $-1$  (red counter-clockwise or blue clockwise arrows in figure 1)<sup>41</sup>.

The Haldane model of honeycomb lattice shows that a non-trivial topology can exist when TR symmetry is broken. The KM model can be considered as spinful Haldane model, composed of two decoupled Hamiltonians, there up and down spin electrons exhibit helical quantum Hall effects in graphene, and backscattering are forbidden due to TR invariance<sup>42</sup>. The band structure of a ZGNR with KM interaction shows that there are two bands which traverse the bulk gap, connecting the  $K$  and  $K'$  points. These bands are localized edge states. The exotic edge states are helical, which propagate in both directions in each band. There, electrons with opposite spin propagate in opposite directions, leading to the spin filtered states<sup>28</sup>. However, a pair of counterpropagating edge modes at each edge can acquire a gap in the presence of large  $\lambda_{SO}$  in KM model<sup>29</sup>. As a result, this system needs further  $Z_2$  topological classification. It is shown that system with KM and Rashba interaction in the presence of magnetic fields shows the QAH phase with Chern number  $C = 2$ <sup>44</sup>. Furthermore, the above model was shown to exhibited equivalent mathematical structure to a spin singlet  $d+id$  superconductor via a duality mapping<sup>45</sup>.

## C. Possible superconducting states in graphene-based materials

For graphene without SO coupling, it has been shown that the superconducting state is of  $d+id$  spin singlet pairing at low energy. By examining the superconducting order on  $K$  and  $K'$  points,  $s$ -wave and exotic  $p+ip$ -wave pairing orders emerge, indicating that  $d+id$ -wave pairing is a mixed state from these two orders<sup>26</sup>. For graphene with KM interaction in stripe geometry, the system is found to also exhibit chiral singlet  $d+id$ -wave superconductivity near half-filling under TR symmetry breaking via a renormalized mean-field approach to the  $t - J$  model. For strong KM interaction, despite the TR symmetry breaking  $d + id'$  superconducting state, helical MFs in 2D spin-singlet topological superconducting state are still found, protected by a pseudo-spin symmetry. With decreasing KM interaction, the system undergoes a topological phase transition to a phase with chiral MFs<sup>30</sup>. To go a step further, our focus here is

to study possible superconducting states when both KM and Rashba terms are present. We search for possible co-existing phase between singlet  $d+id$ - and triplet  $p+ip$ -wave superconductivity.

We now discuss mechanism of possible triplet  $p+ip$ -wave superconductivity on honeycomb lattice. The superconducting pairing on honeycomb lattice has been proposed to exist between electrons on NN sites. The three amplitudes of the superconducting pairing gaps along the three unit lattice vectors are defined as:  $(1, e^{i2\pi/3}, e^{i4\pi/3})$  for  $d+id$ -wave pairing,  $(-2, 1, 1)$  and  $(0, 1, -1)$  for  $p+ip$ -wave pairing (see shaded yellow triangle in figure 1)<sup>49</sup>, which has already been revealed in RVB order parameter<sup>53</sup>. Notice that the spin triplet  $p+ip$ -wave amplitude comes from the linear combination of two components in irreducible representation  $E_2$ <sup>51,52</sup>.

The spin triplet  $p+ip$ -wave pairing symmetry in honeycomb lattice is linked to the Rashba coupling. In Ref.<sup>53</sup>, the Hamiltonian for superconducting graphene, including nearest-neighbor hopping and an Resonating-Valence-Bond (RVB) interaction term, is treated at a mean-field level. In general, it was found that the pairing amplitude along NN direction is  $(1, 1, 1)$  for  $s$  wave pairing,  $(0, -1, 1)$  and  $(2, -1, -1)$  for  $d_{xy}/p_x$  and  $d_{x^2-y^2}/p_y$  pairing state, respectively. Moreover, the complex linear combination of  $d/p$  vectors leading to the  $d+id$ - $p+ip$ -pairing state<sup>49</sup>. It can be seen that, the component of the Rashba term in three different hopping directions shown in Eq. (2) is proportional to that of  $p_x/p_y$  pairing state with odd parity symmetry. They are to be combined to form the  $p+ip$  pairing state due to the Rashba interaction itself. In addition, previous studies show that the spin-triplet component is aligned with the Rashba coupling through the linearized gap equation<sup>22,58</sup>. It has also been shown that the triplet pairing is enhanced by increasing the Rashba coupling<sup>54</sup>: the amplitude of triplet pairing state with  $S^z = \pm 1$  component dominates in the large Rashba coupling regime, confirming that the Rashba coupling favours spin-triplet superconductivity. These developments form a basis for our further investigation on NCS in graphene-based materials.

The general bulk Hamiltonian with  $d + p$  mixed pairing symmetry we consider includes a nearest hopping term ( $H_t$ ), KM interaction ( $H_{KM}$ ), Rashba interaction ( $H_R$ ), the mixing singlet  $d+id$ -wave and triplet  $p+ip$ -wave pairing ( $H_\Delta$ ), chemical potential term ( $H_\mu$ ), and Zeeman coupling term ( $H_B$ ). In momentum space, the model Hamiltonian of the system is written as  $H = H_t + H_{KM} + H_R + H_\mu + H_B + H_\Delta$ , with

$$\begin{aligned}
H_t &= t \sum_{k\sigma} g_k a_{k\sigma}^\dagger b_{k\sigma} + h.c., \\
H_{KM} &= \lambda_{SO} \sum_{k\sigma} \gamma_k \sigma_z \left( a_{k\sigma}^\dagger a_{k\sigma} - b_{k\sigma}^\dagger b_{k\sigma} \right), \\
H_R &= \lambda_R \sum_{k\sigma\sigma'} \tilde{R}_k \cdot \tilde{\sigma} a_{k\sigma}^\dagger b_{k\sigma'} + h.c., \\
H_\mu &= \mu \sum_{k\sigma} \left( a_{k\sigma}^\dagger a_{k\sigma} + b_{k\sigma}^\dagger b_{k\sigma} \right), \\
H_B &= \mu_B B_z \sum_{k\sigma} \sigma_z \left( a_{k\sigma}^\dagger a_{k\sigma} + b_{k\sigma}^\dagger b_{k\sigma} \right), \\
H_\Delta &= \frac{1}{2} \sum_{k\sigma\sigma'} \left[ \Delta(k) a_{k\sigma}^\dagger b_{k\sigma'}^\dagger + \Delta^*(k) a_{-k\sigma} b_{k\sigma'} \right].
\end{aligned} \tag{4}$$

Here  $k = (k_x, k_y)$ , and  $t, \mu$  are the NN hopping parameter and chemical potential, respectively. The magnetic field  $B_z$  is in the  $z$  direction, which results in the Zeeman coupling ( $\mu_B B_z$ ). In what follows we set  $t = 1$ . The  $k$ -dependent NN hopping amplitude, KM and Rashba couplings are given by

$$\begin{aligned}
g_k &= \sum_{l=1}^3 e^{ik \cdot e_l}, \\
\gamma_k &= \sum_{l=1}^6 e^{i(k \cdot e'_l + l\pi + \pi/2)}, \\
\tilde{R}_k &= \sum_{l=1}^3 (-e_{l,y}, e_{l,x}) e^{i(k \cdot e_l + \pi/2)},
\end{aligned} \tag{5}$$

where  $e_l = (e_{l,x}, e_{l,y})$ .  $e'_l$  are NNN vectors, given by  $e'_{1,2} = \pm a_1$ ,  $e'_{3,4} = \mp a_2$ , and  $e'_{5,6} = \pm(a_2 - a_1)$ . The gap function can be represented as  $\Delta(k) = i\Delta_d \sigma_y + i\Delta_t \tilde{R}_k \cdot \tilde{\sigma} \sigma_y$  for the general co-existing singlet ( $d+id$ -wave) and triplet ( $p+ip$ -wave) pairing state, while  $\Delta_d$  and  $\Delta_t$  are the corresponding parameters, respectively. In the Nambu basis, the Hamiltonian Eq. (4) takes the form  $H = \sum_k \psi^\dagger \tilde{h}(k) \psi$ , where

$$\psi^\dagger = \left( a_{k\uparrow}^\dagger \quad b_{k\uparrow}^\dagger \quad a_{k\downarrow}^\dagger \quad b_{k\downarrow}^\dagger \quad a_{-k\uparrow} \quad b_{-k\uparrow} \quad a_{-k\downarrow} \quad b_{-k\downarrow} \right). \tag{6}$$

The  $8 \times 8$  matrix  $\tilde{h}(k)$  reads

$$\tilde{h}(k) = \begin{pmatrix} \tilde{h}_{k,k} & \tilde{h}_{-k,k} \\ \tilde{h}_{k,-k} & \tilde{h}_{-k,-k} \end{pmatrix}, \tag{7}$$

with

$$\tilde{h}_{k,k} = \begin{pmatrix} \gamma'_k - \mu_- & -g_k & 0 & -\lambda_R R_{-k} \\ -g_k^* & -\gamma'_k - \mu_- & \lambda_R R_k & 0 \\ 0 & \lambda_R R_k^* & -\gamma'_k - \mu_+ & -g_k \\ -\lambda_R R_{-k}^* & 0 & -g_k^* & \gamma'_k - \mu_+ \end{pmatrix}, \tag{8}$$

$$\tilde{h}_{k,-k} = \begin{pmatrix} \gamma'_k + \mu_- & -g_k & 0 & \lambda_R R_k^* \\ -g_k^* & -\gamma'_k + \mu_- & -\lambda_R R_{-k}^* & 0 \\ 0 & -\lambda_R R_{-k} & -\gamma'_k + \mu_+ & -g_k \\ \lambda_R R_k & 0 & -g_k^* & \gamma'_k + \mu_+ \end{pmatrix}, \tag{9}$$

$$\tilde{h}_{-k,k} = \begin{pmatrix} 0 & \Delta_t R_{-k} & 0 & \Delta_d L_k \\ -\Delta_t R_k & 0 & \Delta_d L_{-k} & 0 \\ 0 & -\Delta_d L_k & 0 & \Delta_t R_k^* \\ -\Delta_d L_{-k} & 0 & -\Delta_t R_{-k}^* & 0 \end{pmatrix}, \tag{10}$$

$$\tilde{h}_{k,-k} = \begin{pmatrix} 0 & -\Delta_t R_k^* & 0 & -\Delta_d L_{-k}^* \\ \Delta_t R_{-k}^* & 0 & -\Delta_d L_k^* & 0 \\ 0 & \Delta_d L_{-k}^* & 0 & -\Delta_t R_{-k} \\ \Delta_d L_k^* & 0 & \Delta_t R_k & 0 \end{pmatrix}. \tag{11}$$

Then, the matrix elements of the Hamiltonian can be written as

$$\begin{aligned}
L_k &= \sum_{l=1}^3 e^{i[k \cdot e_l + 2\pi(l-1)/3]}, \\
R_k &= -e^{ik_x} + e^{-ik_x/2} \left[ \cos\left(\frac{\sqrt{3}k_y}{2}\right) - \sqrt{3} \sin\left(\frac{\sqrt{3}k_y}{2}\right) \right], \\
\gamma'_k &= \lambda_{SO} \gamma_k, \\
\mu_\pm &= \mu \pm \mu_B B_z.
\end{aligned} \tag{12}$$

Here  $L_k$  and  $R_k$  are  $k$ -components of the Fourier transformed  $d+id$ -wave and  $p+ip$ -wave pairing gaps, respectively.  $\mu_\pm$  is the modified chemical potential of spin up and down electrons. In two dimensional system, inversion and TR symmetries give rise to gapless Dirac modes since these symmetries enforce the  $\sigma_z$  terms vanish in the Hamiltonian<sup>43</sup>. For matrix  $\tilde{h}(k)$ , KM model shows TR symmetry, whereas  $d+id$  and  $p+ip$ -wave order parameters, and Rashba SO interaction break the TR symmetry. In addition, the Rashba coupling and  $p+ip$ -wave order parameters break inversion symmetry<sup>30,31</sup>.

To simplify complex bulk Hamiltonian with Rashba interaction, the author in Ref.<sup>27</sup> takes symmetric and antisymmetric combinations of operators  $a(a^\dagger)$  and  $b(b^\dagger)$  as new band operators. The resulting Hamiltonian is composed of lower and upper  $\pi$  band. The lower band Bogoliubov-de Gennes (BdG) Hamiltonian can be diagonalized through standard Bogoliubov transformation to determine the electronic structure of Fermi surface.

#### D. Chern number calculation

To search for edge modes, the Chern number (Hall conductance) of the system with periodic boundary conditions (bulk) is considered. The Chern number is obtained by integrating Berry curvature over all occupied bands in first Brillouin zone (BZ), can be expressed in the form<sup>55,56</sup>

$$C = \frac{-1}{\pi} \int \int dk_x dk_y \sum_{E_\alpha < 0 < E_\beta} \frac{\text{Im} \langle \alpha | \partial_{k_x} \tilde{h}(k) | \beta \rangle \langle \beta | \partial_{k_y} \tilde{h}(k) | \alpha \rangle}{(E_\alpha - E_\beta)^2}, \tag{13}$$

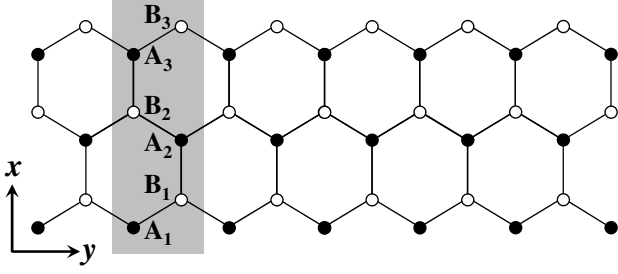


FIG. 2. Schematic plot for a zigzag ribbon. This system shows translational symmetry along  $y$  axis. The gray shaded region represents for the super unit cell. Here, there are three zigzag chains along  $x$  axis, denoted as 3-ZNR. Each super unit cell is composed of six sites,  $A_{1,2,3}$  and  $B_{1,2,3}$  for sublattice A and B, respectively.

where  $\alpha$  and  $\beta$  denote the quasiparticle bands, and  $C$  is the charge Chern number. Note that in the presence of a finite magnetic field and Rashba coupling,  $S^z$  is not a good quantum number<sup>57</sup>. Thus, above equation is not suitable for describing the spin Chern number. Other approaches are needed, which go beyond the scope of this paper.

### E. Hamiltonian matrix of finite system

In principle, the edge states connect bulk bands inside the band gap, and the number of edge modes is equal to the sum of the Chern numbers of each band below Fermi level. To analyze edge modes of the honeycomb lattice, a ZNR is considered. The Hamiltonian matrix is diagonalized directly to obtain band structure. For simplicity, the Hamiltonian matrix for a 3-ZNR within this formalism is given below. This can be straightforwardly extended to ZNR with different widths.

The quantum many body state can be written in the following basis:

$$\Phi^\dagger = \left( \phi_{k\uparrow}^\dagger \quad \phi_{k\downarrow}^\dagger \quad \phi_{-k\uparrow} \quad \phi_{-k\downarrow} \right), \quad (14)$$

each substate passes through either A or B sites of all zigzag chains (see figure 2), reads  $\phi = (A_1 \ B_1 \ A_2 \ B_2 \ A_3 \ B_3)^{41}$ . Hence the Hamiltonian matrix in this basis has the form

$$\tilde{H} = \begin{pmatrix} \tilde{H}_{k\uparrow,k\uparrow} & \tilde{H}_{k\downarrow,k\uparrow} & \tilde{H}_{-k\uparrow,k\uparrow} & \tilde{H}_{-k\downarrow,k\uparrow} \\ \tilde{H}_{k\uparrow,k\downarrow} & \tilde{H}_{k\downarrow,k\downarrow} & \tilde{H}_{-k\uparrow,k\downarrow} & \tilde{H}_{-k\downarrow,k\downarrow} \\ \tilde{H}_{k\uparrow,-k\uparrow} & \tilde{H}_{k\downarrow,-k\uparrow} & \tilde{H}_{-k\uparrow,-k\uparrow} & \tilde{H}_{-k\downarrow,-k\uparrow} \\ \tilde{H}_{k\uparrow,-k\downarrow} & \tilde{H}_{k\downarrow,-k\downarrow} & \tilde{H}_{-k\uparrow,-k\downarrow} & \tilde{H}_{-k\downarrow,-k\downarrow} \end{pmatrix}, \quad (15)$$

where submatrices take the following form:

$$\begin{aligned} \tilde{H}_{k\uparrow,k\uparrow} &= \tilde{H}_t + \tilde{H}_{KM} - \tilde{H}_\mu + \tilde{H}_B, \\ \tilde{H}_{k\downarrow,k\downarrow} &= \tilde{H}_t + \tilde{H}_{KM} (\lambda_{SO} \rightarrow -\lambda_{SO}) - \tilde{H}_\mu - \tilde{H}_B, \\ \tilde{H}_{-k\uparrow,-k\uparrow} &= -\tilde{H}_t - \tilde{H}_{KM} (\lambda_{SO} \rightarrow -\lambda_{SO}) + \tilde{H}_\mu + \tilde{H}_B, \\ \tilde{H}_{-k\downarrow,-k\downarrow} &= -\tilde{H}_t - \tilde{H}_{KM} + \tilde{H}_\mu - \tilde{H}_B, \\ \tilde{H}_{k\downarrow,k\uparrow} &= \tilde{H}_R, \\ \tilde{H}_{k\uparrow,k\downarrow} &= \tilde{H}_{k\downarrow,k\uparrow} (\gamma_1 \rightarrow -\gamma_1), \\ \tilde{H}_{-k\downarrow,-k\uparrow} &= \tilde{H}_{k\uparrow,k\downarrow}, \\ \tilde{H}_{-k\uparrow,-k\downarrow} &= \tilde{H}_{k\downarrow,k\uparrow}, \\ \tilde{H}_{k\downarrow,-k\downarrow} &= \tilde{H}_{\Delta_t}, \\ \tilde{H}_{k\uparrow,-k\uparrow} &= -\tilde{H}_{k\downarrow,-k\downarrow} (\gamma_1 \rightarrow -\gamma_1), \\ \tilde{H}_{-k\downarrow,k\downarrow} &= \tilde{H}_{k\downarrow,-k\downarrow}^\dagger, \\ \tilde{H}_{-k\uparrow,k\uparrow} &= \tilde{H}_{k\uparrow,-k\uparrow}^\dagger, \\ \tilde{H}_{k\uparrow,-k\downarrow} &= \tilde{H}_{\Delta_d}, \\ \tilde{H}_{k\downarrow,-k\uparrow} &= -\tilde{H}_{k\uparrow,-k\downarrow}, \\ \tilde{H}_{-k\downarrow,k\uparrow} &= \tilde{H}_{k\uparrow,-k\downarrow}^\dagger, \\ \tilde{H}_{-k\uparrow,k\downarrow} &= \tilde{H}_{k\downarrow,-k\uparrow}^\dagger, \end{aligned}$$

with

$$\tilde{H}_t = \begin{pmatrix} 0 & t\alpha & & & & \\ t\alpha & 0 & t & & & \\ & t & 0 & t\alpha & & \\ & & t\alpha & 0 & t & \\ & & & t & 0 & t\alpha \\ & & & & t\alpha & 0 \end{pmatrix}, \quad (16)$$

$$\tilde{H}_{KM} = \begin{pmatrix} -\beta_2 & 0 & -\beta_1 & & & \\ 0 & \beta_2 & 0 & \beta_1 & & \\ -\beta_1 & 0 & -\beta_2 & 0 & -\beta_1 & \\ & \beta_1 & 0 & \beta_2 & 0 & \beta_1 \\ & & -\beta_1 & 0 & -\beta_2 & 0 \\ & & & \beta_1 & 0 & \beta_2 \end{pmatrix}, \quad (17)$$

$$\tilde{H}_R = \begin{pmatrix} 0 & \lambda_R \gamma' & & & & \\ \lambda_R \gamma'' & 0 & \lambda_R \gamma & & & \\ & -\lambda_R \gamma & 0 & \lambda_R \gamma' & & \\ & & \lambda_R \gamma'' & 0 & \lambda_R \gamma & \\ & & & -\lambda_R \gamma & 0 & \lambda_R \gamma' \\ & & & & \lambda_R \gamma'' & 0 \end{pmatrix}, \quad (18)$$

$$\tilde{H}_{\Delta_d} = \begin{pmatrix} 0 & \Delta_{12} & & & & \\ \Delta_{12} & 0 & \Delta_0 & & & \\ & \Delta_0 & 0 & \Delta_{12} & & \\ & & \Delta_{12} & 0 & \Delta_0 & \\ & & & \Delta_0 & 0 & \Delta_{12} \\ & & & & \Delta_{12} & 0 \end{pmatrix}, \quad (19)$$

$$\tilde{H}_{\Delta_t} = \tilde{H}_R (\lambda_R \rightarrow \Delta_t), \quad (20)$$

$$\tilde{H}_B = \mu_B B_z \tilde{I}, \quad (21)$$

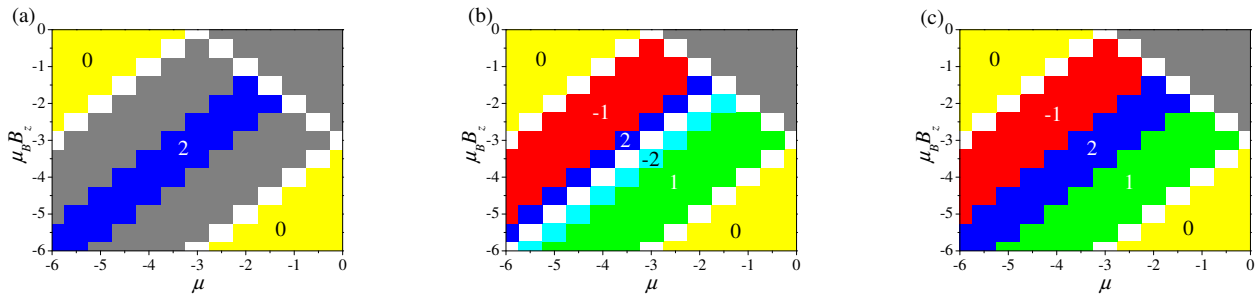


FIG. 3. Topological phase diagram for different pairing states. (a) Singlet:  $\lambda_R = 0$ ,  $\Delta_t = 0$ ,  $\Delta_d = -0.33$ ,  $\lambda_{SO} = 0.143$ . (b) Triplet:  $\lambda_R = 0.33$ ,  $\Delta_t = 0.33$ ,  $\Delta_d = 0$ ,  $\lambda_{SO} = 0$ . (c) Singlet-Triplet Mixing:  $\lambda_R = 0.33$ ,  $\Delta_t = 0.33$ ,  $\Delta_d = -0.33$ ,  $\lambda_{SO} = 0.143$ . Numbers shown in colored areas refer to the corresponding Chern numbers. For unlabeled regions, white (grey) areas represent systems with zero (nearly zero) gap where Chern numbers show crossover behaviors in these regions.

$$\tilde{H}_\mu = \mu \tilde{I}. \quad (22)$$

Blank entries in above matrices are zeros and  $\tilde{I}$  represents unit matrix. The matrix elements are then given by the following expressions:

$$\begin{aligned} \alpha &= 2 \cos(\sqrt{3}k/2), \\ \beta_1 &= 2\lambda_{SO} \sin(\sqrt{3}k/2), \beta_2 = -2\lambda_{SO} \sin(\sqrt{3}k), \\ \gamma_1 &= i\sqrt{3} \sin(\sqrt{3}k/2), \gamma_2 = i \cos(\sqrt{3}k/2), \\ \gamma' &= \gamma_1 - \gamma_2, \gamma'' = \gamma_1 + \gamma_2, \gamma = i, \\ \Delta_0 &= \Delta_d, \Delta_1 = \Delta_d e^{i2\pi/3}, \\ \Delta_2 &= \Delta_d e^{i4\pi/3}, \Delta_{12} = \Delta_1 + \Delta_2. \end{aligned} \quad (23)$$

Here  $k = k_y$ , and  $\Delta_{i=0,1,2}$  are the matrix elements of  $d+id$ -wave pairing in ZGNR system<sup>30</sup>. The eigenvectors,  $\Psi$ , corresponding to Hamiltonian matrix Eq. (15) have the form

$$\Psi = (\Psi_{k\bar{\uparrow}}, \Psi_{k\bar{\downarrow}}, \Psi_{-k\bar{\uparrow}}, \Psi_{-k\bar{\downarrow}})^T, \quad (24)$$

where  $\Psi_{\pm k\bar{\sigma}=\bar{\uparrow},\bar{\downarrow}} = \Psi_{\pm k\bar{\sigma}=\bar{\uparrow},\bar{\downarrow}}(x; A', B')$ . Here,  $x$ ,  $\bar{\sigma}$  and  $A'(B')$  are position across the ribbon (see figure 2), quasiparticle and sublattice pseudospin, respectively. Note that, the quasiparticle pseudospin indices  $\bar{\sigma} = \bar{\sigma}(\bar{\uparrow}, \bar{\downarrow})$  are linear combination of original up and down spin states.

### III. RESULTS

#### A. General bulk topological phase diagram

The NCS supports MF zero energy modes at the edge of vortex cores in the presence of a magnetic field<sup>22</sup>. To study possible topological phases and phase transitions, we first examine the topology of bulk band by computing Chern numbers ( $C$ ). The gap closing condition is used in the bulk spectrum to determine distinct topological nature<sup>27</sup>. Topologically non-trivial systems carry

nonzero Chern numbers. Via bulk-edge correspondence, non-trivial bulk Chern number indicates the number of edge states. The sign of Chern number indicates the curvature of the Fermi surface or the chirality of the bulk band gap function<sup>22</sup>.

The topological phase diagrams as a function of the chemical potential ( $\mu$ ) and Zeeman coupling ( $\mu_B B_z$ ) are presented in figure 3. We consider three cases: (i) finite KM coupling and spin singlet  $d+id$ -wave pairing (see figure 3(a)) (ii) finite Rashba coupling and spin triplet  $p+ip$ -wave pairing (see figure 3(b)) and (iii) mixture of above two cases (see figure 3(c)).

The phase diagram for system at a finite Zeeman coupling is shown in figure 3(a). The gap closing points (white region) divide the phase diagram into several

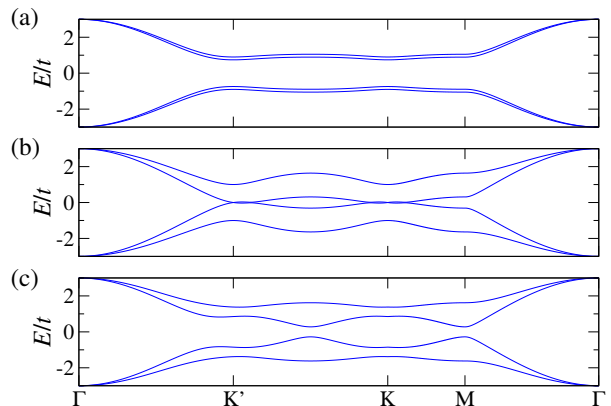


FIG. 4. Dispersion relation of a bulk system along different high symmetry points (only states close to zero energy are shown). We take  $t = 1$ ,  $\mu = -3$ ,  $\mu_B B_z = -3$  for (a) singlet pairing:  $\Delta_d = -0.33$ ,  $\lambda_{SO} = 0.143$ ,  $\lambda_R = 0$ ,  $\Delta_t = 0$ . (b) triplet pairing:  $\Delta_d = 0$ ,  $\lambda_{SO} = 0$ ,  $\lambda_R = 0.33$ ,  $\Delta_t = 0.33$ . (c) mixing:  $\Delta_d = -0.33$ ,  $\lambda_{SO} = 0.143$ ,  $\lambda_R = 0.33$ ,  $\Delta_t = 0.33$ .

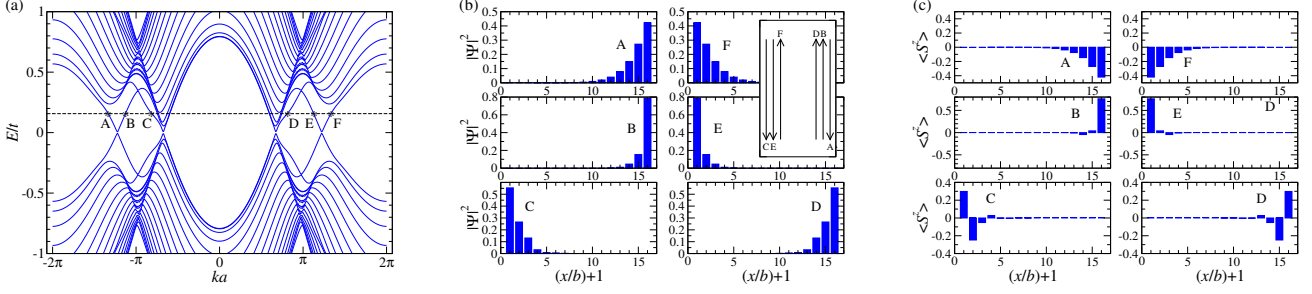


FIG. 5. (a) Band structure of a 16-ZNR for  $\lambda_R = 0.3$ ,  $\Delta_t = 0.3$ ,  $\Delta_d = -0.3$ ,  $\lambda_{SO} = 0.13$ ,  $\mu = -3.41$ ,  $\mu_B B_z = -2.95$ . The magnitude of parameters are similar to those of bulk in figure 3(c). The Fermi level is indicated by the dashed horizontal line above zero energy, and the intersections with the edge state dispersion are denoted by capital letters ("\*"). Small gaps in the edge states are due to finite-size effects<sup>27</sup>. (b) Edge state probability, charge current (inset) distributions. The arrows in inset describe the propagating directions of charge currents. (c) Spin polarization as a function of position across the ZNR. The amplitude square of edge state wave functions exhibits exponential decay from both edges into the bulk. Here, one chiral (C, D) and one pair of helical edge modes, (A, F) and (B, E), emerge. Due to the influence of edge mode (C, D), B and E are not purely spin filtered edge states.

parts. The Chern number is zero in the yellow region, indicating trivial band insulators. The off-diagonal region (blue area) shows Chern number  $C = 2$ . This result is similar to that for a chiral superconductor without Zeeman couplings<sup>45</sup>. The grey area indicates fluctuating Chern numbers, which may lie near the phase boundaries. The phase diagram for bulk system with Rashba interaction and  $p+ip$ -wave spin triplet pairing is shown in

figure 3(b). Similar result has been found in the square lattice with the same set of interactions<sup>22</sup>.

It has been shown that KM interaction opens up a gap at the Dirac points in graphene<sup>29</sup>. Therefore, the main effect of KM interaction is lifting degeneracy of the bulk band. This enables us to calculate Chern number at gap closing points. Based on the same parameters used in figure 3(a) and (b), we consider system with all couplings being finite in the figure 3(c).

Figure 4 shows the bulk energy bands, corresponding to the central point ( $\mu = \mu_B B_z = -3$ ) in topological phase diagrams of figure 3. In the case of KM and  $d+id$ -wave pairing (see figure 4(a)), flat and gapped bands appear around high symmetry points (see figure 3(a)). In the case of Rashba and  $p+ip$ -wave superconductivity (see figure 4(b)), each of the degenerate bands splits into two, and band touching occurs at  $K$  and  $K'$  points (see figure 3(b)). Figure 4(c) shows the co-existence of singlet-triplet pairing (see figure 3(c)). A mixture of chiral and helical edge states in the finite-size ZNRs is found. We will analyze the energy spectra of ZNRs in the following section.

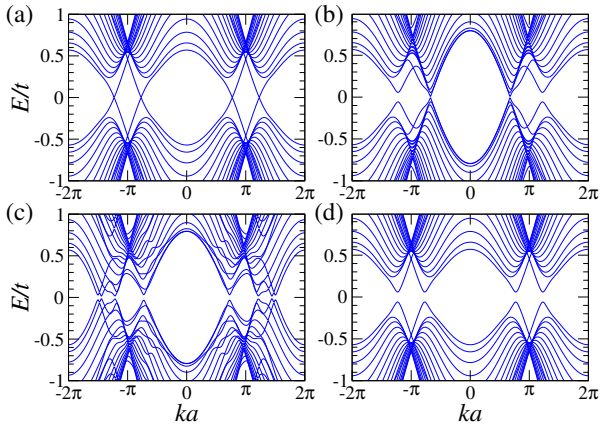


FIG. 6. Band structure of a 16-ZNR for different setting from figure 5(a). (a)  $\lambda_R = 0$ ,  $\Delta_t = 0$ ,  $\Delta_d = 0$ ,  $\lambda_{SO} = 0.13$ ,  $\mu = -3.41$ ,  $\mu_B B_z = -2.95$ . (b)  $\lambda_R = 0$ ,  $\Delta_t = 0$ ,  $\Delta_d = -0.3$ ,  $\lambda_{SO} = 0.13$ ,  $\mu = -3.41$ ,  $\mu_B B_z = -2.95$ . (c)  $\lambda_R = 0.3$ ,  $\Delta_t = 0.3$ ,  $\Delta_d = -0.3$ ,  $\lambda_{SO} = 0$ ,  $\mu = -3.41$ ,  $\mu_B B_z = -2.95$ . (d)  $\lambda_R = 0.3$ ,  $\Delta_t = 0.3$ ,  $\Delta_d = 0$ ,  $\lambda_{SO} = 0.13$ ,  $\mu = -3.41$ ,  $\mu_B B_z = -2.95$ . These figures show the band structure shown in figure 5(a) exists for a variety choices of parameters in our model.

## B. Band structures and edge states of ZNRs

To confirm the emergence of edge mode in sample boundary with non-trivial bulk Chern number, band structures of a finite sized ZNR with periodic boundary conditions in the  $y$ -direction are considered (see figure 2). In the normal state of graphene, a pair of gapless counterpropagating helical edge modes exist when KM interaction dominates<sup>28</sup>. On the other hand, the Rashba coupling leads to co-propagating chiral edge modes in the ZGNR spectrum<sup>44</sup>. When KM and Rashba interac-

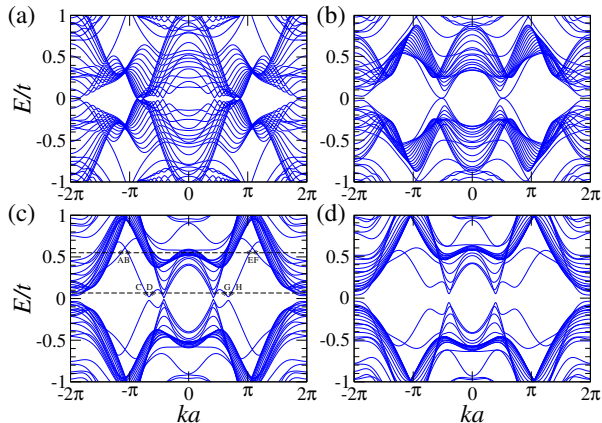


FIG. 7. Band structure of a 16-ZNR for  $\lambda_R = 0.3$ ,  $\Delta_d = -0.3$ ,  $\lambda_{SO} = 0.13$ ,  $\mu = -0.5$ ,  $\mu_B B_z = -1.5$ . (a)  $\Delta_t = 0$ . (b)  $\Delta_t = 0.3$ . (c)  $\Delta_t = 0.6$ . (d)  $\Delta_t = 0.75$ . In (c), edge states are denoted in the same way as shown in figure 5(a). The system undergoes a topological phase transition to a topologically non-trivial phase as  $\Delta_t$  is increased, and returns back to a topologically trivial phase at large  $\Delta_t$ .

tion are both present, topological phase transitions can be induced under staggered sublattice potential<sup>29</sup> or exchange field<sup>61</sup>. In the superconducting states, however, the topological non-trivial edge states are zero-energy self-conjugate MFs. The chiral and helical MF modes can be supported by either KM or Rashba interaction<sup>27,30</sup>.

The topological band structure of a 16-ZNR is shown in figure 5(a). Figure 5(b) shows the corresponding edge state wave functions and charge current distributions,  $|\Psi|^2 = |\Psi_{\pm k\uparrow}|^2 + |\Psi_{\pm k\downarrow}|^2$ . Figure 5(c) shows the spin polarization of each edge state, defined as  $\langle S^z \rangle = |\Psi_{\pm k\uparrow}|^2 - |\Psi_{\pm k\downarrow}|^2$ <sup>40,61</sup>. It appears that there are paired (A, F), (B, E) and unpaired (C, D) edge states in figure 5. The three edge states A, B and D are on the same edge, and C, E and F states on the other edge (see figure 5(b)). As shown in Figure 5(c), the paired edge states (A, F) and (B, E) belong to counter propagating helical modes. The unpaired (C, D) edge states are co-propagating chiral modes. The oscillation of spin polarization on unpaired edge state is similar to that found on ZGNR with Rashba interaction<sup>40</sup>, indicating that this unpaired edge state comes from triplet pairing. Charge current distributions on each edge correspond to the bulk topological phase with  $|C| = 1$ <sup>61</sup>. Note that, parameters used here are slightly different from that in the bulk phase diagram. We think this discrepancy is originated from the difference in topologies of mobile  $\pi$  electrons between finite and infinite systems<sup>63</sup>. As a result, magnitude of parameters, such as NN and NNN hopping integrals, are not the same in both cases<sup>64</sup>.

We have systematically varied the parameter setting

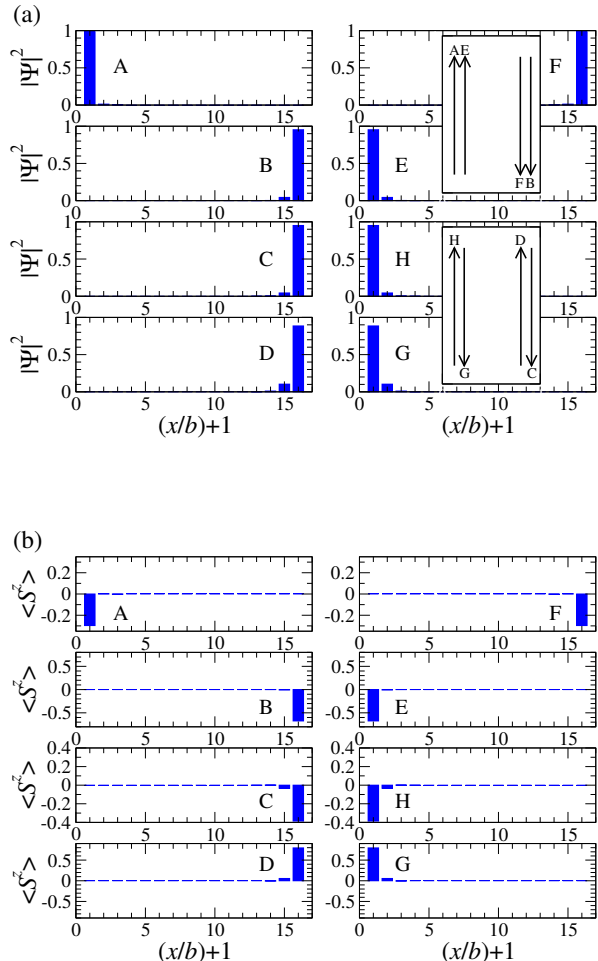


FIG. 8. (a) Schematic plot of edge state probability for chiral (upper inset), helical (lower inset) edge states and (b) Spin polarization of figure 7(c). Edge states (A, B, E, F) and (C, D, G, H) are associated with the intersections with the upper and lower dashed horizontal lines in figure 7(c), respectively.

used in figure 5(a), and the same parameters are used in figure 6. We find Dirac cones crossing the band gap to appear in the presence of KM interaction. The band structure shown in figure 6(a) indicates that non-vanishing  $\mu$  and  $\mu_B B_z$  jointly induce TR symmetry breaking. Each of the two Dirac cones splits into two around zone boundary  $k = \pm\pi/a$ . However, we find the chiral unpaired edge state (C, D in figure 5(a)) can also come from singlet  $d+id$  state with TR symmetry breaking (see figure 6(b)).

To elucidate the topological phase transition for different  $\Delta_t$ , we plot the corresponding band structures in figure 7. For  $\Delta_t = 0$ , we find no topologically edge states (see figure 7(a)). However, the system undergoes topological phase transition as  $\Delta_t$  is increased. In figure 7(b), a single chiral edge mode appears. The situation becomes



more complicated for large  $\Delta_t$  (for example,  $\Delta_t = 2\lambda_R$  in figure 7(c)). There are two kinds of edge states appearing: upper (A, B, E, F) states at finite energy and lower (C, D, G, H) edge states at low energy close to zero. As shown in figure 8, the lower edge states consist of a pair of counter propagating modes. Each edge contains spin filtered currents. Two edge states G and H are on the same edge, and so are the C and D states. The upper edge states belong to co-propagating chiral edge mode at finite energies. Two edge states A and E are on the same edge, and so are the F and B states. The spin polarization is the same for all states, which is similar to figure 5(c). Finally, the topological phase disappears at sufficiently large  $\Delta_t$  (see figure 7(d)).

## IV. DISCUSSIONS

### A. Model comparisons

It has been shown theoretically that MFs may appear in graphene. The  $d+id$  pairing superconducting graphene hosts two chiral edge states in ZGNR, MFs will be created at single edge mode in the presence of Rashba interaction and a moderate Zeeman coupling<sup>27</sup>. Meanwhile,  $d+id$  superconductivity in graphene also supports helical Majorana modes in the presence of KM interaction<sup>30</sup>.

In the present work, we start by considering honeycomb lattice bulk topological phase system with KM interaction and singlet pairing ( $d+id$ -wave) under Zeeman couplings. We further study the phase diagram for system with Rashba interaction induced triplet pairing ( $p+ip$ -wave). It is found the outcomes in the case are similar to that from previous studies<sup>22,45</sup>. When all interactions are included, the phase diagrams show the feature of singlet-triplet mixture.

We then study the edge state behavior of ZNRs in this most interesting case. Our parity mixing model can host three states per edge crossing the bulk gap in a ZNR. We find that helical and chiral Majorana edge modes can exist near Fermi level simultaneously. For large value of  $\Delta_t$  ( $\Delta_t = 2\lambda_R$ ), we also observe chiral edge modes at finite energy, whereas helical edge states still in the vicinity of zero energy.

### B. Duality

Mathematically, there is a duality between a  $s$ -wave system and a chiral  $p+ip$ -wave superconductor when Rashba SO interaction is taken into consideration<sup>62</sup>. This scheme is applied successfully on a  $s$ -wave superfluid of neutral fermionic atoms in the 2D optical square lattice with laser-field-generated effective Rashba SO interactions<sup>62</sup>. Through a unitary transformation, the Hamiltonian with  $s$ -wave pairing and Rashba SO

interaction is mapped into the dual  $p+ip$ -wave Hamiltonian, which exhibits non-trivial topological superconductivity when Zeeman couplings go beyond a critical value<sup>65</sup>. For honeycomb lattice with singlet  $d+id$ -wave pairing and KM interaction, it has been demonstrated that the Hamiltonian is equivalent to a collection of two topological ferromagnetic insulators, as described in Section 2, offers an explanation to why such setup could exhibit chiral edge states<sup>45</sup>.

### C. Correlated honeycomb lattice

Although many fascinating properties of graphene-based system are well described by the low energy Dirac fermions, the electron-electron interactions are still of great interest. The many-body effect in graphene can be induced by doping or electron-electron interaction. The critical  $M$  points in band structure of graphene are associated with the well-known Van Hove singularity, playing a crucial role in the pairing symmetry of correlated graphene. For example, in graphene a spin-triplet  $f$ -wave instability occurs when it is doped to the Van Hove singularity at 1/4 doping<sup>66</sup>. It hosts helical MFs at large SO coupling<sup>30</sup>, and turns into to  $p+ip$ -wave triplet superconductor as interaction strength is increased<sup>49</sup>. However, the issue on pairing symmetry in correlated graphene has not been settled. Different models and computational methods lead to various different results<sup>46-51</sup>. Therefore, it would be interesting to further study various possible effects of electronic correlation on our parity mixing state.

## V. CONCLUSIONS

In this work, we study topological phase diagram and edge states in non-centrosymmetric superconductors on honeycomb lattice with broken inversion symmetry. Due to the lack of inversion symmetry, co-existence between spin-singlet and spin-triplet pairings are in general expected in non-centrosymmetric superconductors. Promising candidates of this kind include: graphene and graphene-based two-dimensional materials. Due to the presence of both Kane-Mele intrinsic and Rashba spin-orbit couplings, the superconducting state shows parity-mixing phases between singlet  $d+id$ -wave and triplet  $p+ip$ -wave pairing states. We compute the topological Chern number in the bulk system and map out the topological phase diagram. We further study the possible edge states on a finite-size ribbon. For strong Kane-Mele intrinsic spin-orbit coupling, the helical Majorana modes are favoured despite the underlying time-reversal symmetry breaking  $d+id$ -wave singlet pairing. In the other limit with strong Rashba spin-orbit coupling, however, the spin-triplet  $p+ip$ -wave pairing is favoured, leading to chiral Majorana fermions at edges. When the strength of the Kane-Mele and the Rashba couplings are compara-

ble, we find in certain parameter regime the co-existence between chiral and helical Majorana fermions at edges, a signature of parity-mixing. Our results provide useful guidance in searching for non-centrosymmetric superconductors on graphene-based materials.

## ACKNOWLEDGMENTS

This work is supported by the MOST Grant No. 104-2112-M-009-004-MY3, the NCTS of Taiwan, R.O.C..

- 
- <sup>1</sup> S. S. Saxena and P. Monthoux, *Nature* **427**, 799 (2004).  
<sup>2</sup> M. Xu, T. Liang, M. Shi, and H. Chen, *Chem. Rev.* **113**, 3766 (2013).  
<sup>3</sup> B. Radisavljevic, A. Radenovic, J. Brivio, V. Giacometti, and A. Kis, *Nat. Nanotechnol.* **6**, 147 (2011).  
<sup>4</sup> Q. H. Wang, K. K. Zadeh, A. Kis, J. N. Coleman, and M. S. Strano, *Nat. Nanotechnol.* **7**, 699 (2012).  
<sup>5</sup> J. T. Ye, Y. J. Zhang, R. Akashi, M. S. Bahramy, R. Arita, Y. Iwasa, *Science*, **338**, 1193 (2012).  
<sup>6</sup> X. Xu, W. Yao, D. Xiao, and T. F. Heinz, *Nat. Phys.* **10**, 343 (2014).  
<sup>7</sup> W. Shi, J. Ye, Y. Zhang, R. Suzuki, M. Yoshida, J. Miyazaki, N. Inoue, Y. Saito, and Y. Iwasa, *Sci. Rep.*, **5**, 12534 (2015).  
<sup>8</sup> J. M. Lu, O. Zheliuk, I. Leermakers, N. F. Q. Yuan, U. Zeitler, K. T. Law, J. T. Ye, *Science*, **350**, 1353 (2015).  
<sup>9</sup> X. Xi, L. Zhao, Z. Wang, H. Berger, L. Forro, J. Shan, and K. F. Mak, *Nat. Nanotechnol.* **10**, 765 (2015).  
<sup>10</sup> X. Xi, Z. Wang, W. Zhao, J. H. Park, K. T. Law, H. Berger, L. Forro, J. Shan, and K. F. Mak, *Nat. Phys.* **12**, 139 (2016).  
<sup>11</sup> Y. Saito, Y. Nakamura, M. S. Bahramy, Y. Kohama, J. Ye, Y. Kasahara, Y. Nakagawa, M. Onga, M. Tokunaga, T. Nojima, Y. Yanase, and Y. Iwasa, *Nat. Phys.* **12**, 144 (2016).  
<sup>12</sup> B. T. Zhou, N. F. Q. Yuan, H. L. Jiang, and K. T. Law, *Phys. Rev. B* **93**, 180501(R) (2016).  
<sup>13</sup> Z. Wang, D. K. Ki, J. Y. Khoo, D. Mauro, H. Berger, L. S. Levitov, and A. F. Morpurgo, *Phys. Rev. X* **6**, 041020 (2016).  
<sup>14</sup> A. Manchon, H. C. Koo, J. Nitta, S. M. Frolov and R. A. Duine, *Nat. Mater.* **14**, 871 (2015).  
<sup>15</sup> M. Ezawa, *Phys. Rev. Lett.* **109**, 055502 (2012).  
<sup>16</sup> H. C. Manoharan, *Nat. Nanotechnol.* **5**, 477 (2010).  
<sup>17</sup> D. Xiao, M. C. Chang and Q. Niu, *Rev. Mod. Phys.* **82**, 1959 (2010).  
<sup>18</sup> M. Z. Hasan and C. L. Kane, *Rev. Mod. Phys.* **82**, 3045 (2008).  
<sup>19</sup> X. L. Qi and S. C. Zhang, *Rev. Mod. Phys.* **83**, 1057 (2011).  
<sup>20</sup> J. Alicea, *Rep. Prog. Phys.* **75**, 076501 (2012).  
<sup>21</sup> M. Hohenadler and F. F. Assaad, *J. Phys.: Condens. Matter* **25**, 143201 (2013).  
<sup>22</sup> M. Sato and S. Fujimoto, *Phys. Rev. B* **79**, 094504 (2009).  
<sup>23</sup> N. F. Q. Yuan, K. F. Mak, and K. T. Law, *Phys. Rev. Lett.* **113**, 097001 (2014).  
<sup>24</sup> Y. Saito, T. Nojima and Y. Iwasa, *Supercond. Sci. Technol.* **29**, 093001 (2016).  
<sup>25</sup> A. M. Black-Schaffer and C. Honerkamp, *J. Phys.: Condens. Matter* **26**, 423201 (2014).  
<sup>26</sup> Y. Jiang, D. X. Yao, E. W. Carlson, H. D. Chen, and J. P. Hu, *Phys. Rev. B* **77**, 235420 (2008).  
<sup>27</sup> A. M. Black-Schaffer, *Phys. Rev. Lett.* **109**, 197001 (2012).  
<sup>28</sup> C. L. Kane and E. J. Mele, *Phys. Rev. Lett.* **95**, 226801 (2005).  
<sup>29</sup> S. Rachel and K. Le-Hur, *Phys. Rev. B* **82**, 075106 (2010).  
<sup>30</sup> S. J. Sun, C. H. Chung, Y. Y. Chang, W. F. Tsai and F. C. Zhang, *Sci. Rep.* **6**, 24102 (2016).  
<sup>31</sup> J. T. Kao, S. M. Huang, C. Y. Mou, and C. C. Tsuei, *Phys. Rev. B* **91**, 134501 (2015).  
<sup>32</sup> T. Yoshida and Y. Yanase, *Phys. Rev. B* **93**, 054504 (2016).  
<sup>33</sup> J. D. Sau, R. M. Lutchyn, S. Tewari, and S. D. Sarma, *Phys. Rev. Lett.* **104**, 040502 (2010).  
<sup>34</sup> J. Alicea, *Phys. Rev. B* **81**, 125318 (2010).  
<sup>35</sup> J. Nilsson, A. R. Akhmerov, and C. W. J. Beenakker, *Phys. Rev. Lett.* **101**, 120403 (2008).  
<sup>36</sup> A. R. Akhmerov, J. Nilsson, and C. W. J. Beenakker, *Phys. Rev. Lett.* **102**, 216404 (2009).  
<sup>37</sup> V. Mourik, K. Zuo, S. M. Frolov, S. R. Plissard, E. P. A. M. Bakkers, and L. P. Kouwenhoven, *Science*, **336**, 1003 (2012).  
<sup>38</sup> S. N. Perge, I. K. Drozdov, J. Li, H. Chen, S. Jeon, J. Seo, A. H. MacDonald, B. A. Bernevig, A. Yazdani, *Science*, **346**, 602 (2014).  
<sup>39</sup> M. Laubach, J. Reuther, R. Thomale, and S. Rachel, *Phys. Rev. B* **90**, 165136 (2014).  
<sup>40</sup> M. Zarea and N. Sandler, *Phys. Rev. B* **79**, 165442 (2009).  
<sup>41</sup> C. H. Chung, D. H. Lee, and S. P. Chao, *Phys. Rev. B* **90**, 035116 (2014).  
<sup>42</sup> C. Z. Chang and M. Li, *J. Phys.: Condens. Matter* **28**, 123002 (2016).  
<sup>43</sup> B. A. Bernevig and T. L. Hughes, *Topological Insulators and Topological Superconductors* (Princeton press, New Jersey, 2013), p. 119.  
<sup>44</sup> Z. Qiao, S. A. Yang, W. Feng, W. K. Tse, J. Ding, Y. Yao, J. Wang, and Q. Niu, *Phys. Rev. B* **82**, 161414 (2010).  
<sup>45</sup> S. M. Huang, W. F. Tsai, C. H. Chung, and C. Y. Mou, *Phys. Rev. B* **93**, 054518 (2016).  
<sup>46</sup> Z. C. Gu, H. C. Jiang, D. N. Sheng, H. Yao, L. Balents, and X. G. Wen, *Phys. Rev. B* **88**, 155112 (2013).  
<sup>47</sup> A. M. Black-Schaffer, W. Wu, and K. Le-Hur, *Phys. Rev. B* **90**, 054521 (2014).  
<sup>48</sup> T. Ma, F. Yang, H. Yao, and H. Q. Lin, *Phys. Rev. B* **90**, 245114 (2014).  
<sup>49</sup> X. Y. Xu, S. Wessel, and Z. Y. Meng, *Phys. Rev. B* **94**, 115105 (2016).  
<sup>50</sup> S. Tsuchiya, J. Goryo, E. Arahata, and M. Sigrist, *Phys. Rev. B* **94**, 104508 (2016).  
<sup>51</sup> J. P. L. Faye, P. Sahebsara, and D. Senechal, *Phys. Rev. B* **92**, 085121 (2015).  
<sup>52</sup> J. P. L. Faye, M. N. Diarra, and D. Senechal, *Phys. Rev. B* **93**, 155149 (2016).  
<sup>53</sup> A. M. Black-Schaffer and S. Doniach, *Phys. Rev. B* **75**, 134512 (2007).  
<sup>54</sup> Y. M. Ru, Master thesis (National Chiao Tung University, Hsinchu, 2017), p. 77.  
<sup>55</sup> J. M. Murray and O. Vafek, *Phys. Rev. B* **92**, 134520 (2015).

- <sup>56</sup> D. J. Thouless, M. Kohmoto, M. P. Nightingale, and M. denNijs, Phys. Rev. Lett. **49**, 405 (1982).
- <sup>57</sup> L. Xu, Y. Zhou and C. D. Gong, J. Phys.: Condens. Matter **25**, 335503 (2013).
- <sup>58</sup> P. A. Frigeri, D. F. Agterberg, A. Koga, and M. Sigrist, Phys. Rev. Lett. **92**, 097001 (2004).
- <sup>59</sup> A. P. Schnyder, S. Ryu, A. Furusaki, and A. W. W. Ludwig, Phys. Rev. B **78**, 195125 (2008).
- <sup>60</sup> X. L. Qi, T. L. Hughes, and S. C. Zhang, Phys. Rev. B **78**, 195424 (2008).
- <sup>61</sup> T. W. Chen, Z. R. Xiao, D. W. Chiou, and G. Y. Guo, Phys. Rev. B **84**, 165453 (2011).
- <sup>62</sup> M. Sato, Y. Takahashi, and S. Fujimoto, Phys. Rev. Lett. **103**, 020401 (2009).
- <sup>63</sup> K. Nakada, M. Fujita, G. Dresselhaus and M. S. Dresselhaus, Phys. Rev. B **54**, 17954 (1996).
- <sup>64</sup> Y. Hancock, A. Uppstu, K. Saloritta, A. Harju, and M. J. Puska, Phys. Rev. B **81**, 245402 (2010).
- <sup>65</sup> M. Sato and S. Fujimoto, J. Phys. Soc. Jpn. **85**, 072001 (2016).
- <sup>66</sup> C. Honerkamp, Phys. Rev. Lett. **100**, 146404 (2008).